Title

Targeting deoxycytidine kinase improves symptoms in mouse models of multiple sclerosis

Journal

Immunology, 168(1)

ISSN

0019-2805

Authors

Chen, Bao Ying

Salas, Jessica R

Trias, Alyssa O

et al.

Publication Date

2023

DOI

10.1111/imm.13569

Peer reviewed

HHS Public Access

Author manuscript

Immunology. Author manuscript; available in PMC 2024 January 01.

Published in final edited form as:

Immunology. 2023 January ; 168(1): 152–169. doi:10.1111/imm.13569.

Targeting deoxycytidine kinase improves symptoms in mouse models of multiple sclerosis

Bao Ying Chen[1,2], **Jessica R. Salas**[1,2], **Alyssa O. Trias**[1,2], **Arely Perez Rodriguez**[1,2], **Jonathan E. Tsang**[1], **Miriam Guemes**[3], **Thuc M. Le**[1,4], **Zoran Galic**[3], **H. Michael Shepard**[5], **Lawrence Steinman**[6], **David A. Nathanson**[1,4], **Johannes Czernin**[1,4], **Owen N. Witte**[1,7,8], **Caius G. Radu**[1,4], **Kenneth A. Schultz**[9], **Peter M. Clark**[1,2,7]

[1]Department of Molecular and Medical Pharmacology, University of California, Los Angeles, Los Angeles, CA, USA

[2]Crump Institute for Molecular Imaging, University of California, Los Angeles, Los Angeles, CA, USA

[3]Department of Medicine, University of California, Los Angeles, Los Angeles, CA, USA

[4]Ahmanson Translational Imaging Division, University of California, Los Angeles, Los Angeles, CA, USA

[5]Enosi Life Sciences, Eugene, OR, USA

[6]Department of Neurology and Neurological Sciences, Stanford University School of Medicine, Stanford, CA, USA

[7]Eli and Edythe Broad Center of Regenerative Medicine and Stem Cell Research, University of California, Los Angeles, Los Angeles, CA, USA

[8]Department of Microbiology, Immunology, and Molecular Genetics, University of California, Los Angeles, Los Angeles, CA, USA

Correspondences should be addressed to: Peter M. Clark, Crump Institute, Box 951770, 4333 CNSI, Los Angeles, CA 90095-1770; 310-267-4755; pclark@mednet.ucla.edu.

Authors' contributions: BYC: Conceptualization, Methodology, Formal analysis, Investigation, Writing – Original Draft, Writing – Review & Editing, Visualization; JRS: Investigation, Writing – Review & Editing; AOT: Investigation, Writing – Review & Editing; APR: Investigation, Writing – Review & Editing; JET: Methodology, Formal analysis, Investigation, Writing – Review & Editing, Visualization; MG: Investigation, Writing – Review & Editing; TML: Methodology, Formal analysis, Investigation, Writing – Review & Editing; ZG: Methodology, Investigation, Writing – Review & Editing; HMS: Conceptualization, Writing – Review & Editing; LS: Conceptualization, Writing – Review & Editing; DAN: Conceptualization, Methodology, Writing – Review & Editing; JC: Conceptualization, Writing – Review & Editing, Funding acquisition; ONW: Conceptualization, Writing – Review & Editing, Funding acquisition; CGR: Conceptualization, Writing – Review & Editing; KAS: Conceptualization, Validation, Formal analysis, Resources, Writing – Original Draft, Writing – Review & Editing, Visualization, Supervision, Project administration, Funding acquisition; PMC: Conceptualization, Validation, Formal analysis, Writing – Original Draft, Writing – Review & Editing, Visualization, Supervision, Project administration, Funding acquisition.

Ethics approval statement: All mouse studies at UCLA were approved of by the UCLA Animal Resource Committee. All mouse experiments at Crown Biosciences and Charles River Laboratories were per their established EAE protocols and complied with local animal welfare guidelines.

Conflict of interest disclosure: ONW currently has consulting, equity, and/or board relationships with Kronos Biosciences, Sofie Biosciences, Breakthrough Properties, Vida Ventures, Nammi Therapeutics, Two River, Iconovir, Appia BioSciences, Neogene Therapeutics, 76Bio, and Allogene Therapeutics. None of these companies contributed to or directed any of the research reported in this article. ONW, JC, and CGR are inventors on patents that disclose [^{18}F]FAC. JC, CGR, and DAN are inventors on patents that disclose TRE-515. PMC, ONW, DAN, JC, CGR, and KAS hold stock shares of Trethera Corporation, which is developing TRE-515. HMS and LS are paid members of the Trethera Corporation Scientific Advisory Board. KAS is an employee of Trethera Corporation.

[9]Trethera Corporation, Sherman Oaks, CA, USA

Abstract

Multiple sclerosis (MS) is an autoimmune disease driven by lymphocyte activation against myelin autoantigens in the central nervous system leading to demyelination and neurodegeneration. The deoxyribonucleoside salvage pathway with the rate-limiting enzyme deoxycytidine kinase (dCK) captures extracellular deoxyribonucleosides for use in intracellular deoxyribonucleotide metabolism. Previous studies have shown that deoxyribonucleoside salvage activity is enriched in lymphocytes and required for early lymphocyte development. However, specific roles for the deoxyribonucleoside salvage pathway and dCK in autoimmune diseases such as MS are unknown. Here we demonstrate that dCK activity is necessary for the development of clinical symptoms in the $MOG_{35–55}$ and $MOG_{1–125}$ experimental autoimmune encephalomyelitis (EAE) mouse models of MS. During EAE disease, deoxyribonucleoside salvage activity is elevated in the spleen and lymph nodes. Targeting dCK with the small molecule dCK inhibitor TRE-515 limits disease severity when treatments are started at disease induction or when symptoms first appear. EAE mice treated with TRE-515 have significantly fewer infiltrating leukocytes in the spinal cord, and TRE-515 blocks activation-induced B and T cell proliferation and $MOG_{35–55}$-specific T cell expansion without affecting innate immune cells or naïve T and B cell populations. Our results demonstrate that targeting dCK limits symptoms in EAE mice and suggest that dCK activity is required for $MOG_{35–55}$-specific lymphocyte activation-induced proliferation.

Graphical Abstract

Identifying new targetable proteins in multiple sclerosis could improve the treatment of this disease. Deoxycytidine kinase is the rate-limiting enzyme in the deoxyribonucleoside salvage pathway. We show that deoxycytidine kinase activity is upregulated in the lymph nodes and spleen in models of multiple sclerosis. Treating these models prophylactically or therapeutically with the dCK inhibitor TRE-515 limits disease. TRE-515 selectively blocks T and B cell activation-induced proliferation without affecting other aspects of the immune system including naïve T and B cells or innate immune cells. Our results suggest deoxycytidine kinase as a potential target for the treatment of multiple sclerosis.

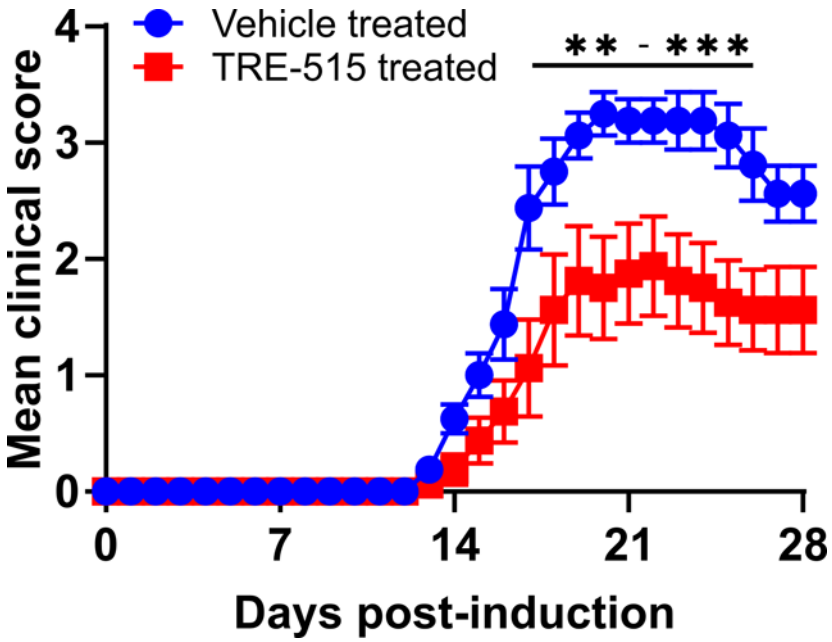

Keywords

Autoimmunity; EAE/MS; Imaging

Introduction:

Multiple sclerosis (MS) is a chronic autoimmune disease in which cells of the immune system attack myelin in the central nervous system (CNS) leading to neuroinflammation, demyelination, and neurodegeneration (1–4). MS pathology is likely driven primarily by T and B lymphocytes that recognize myelin autoantigens (5,6). Most MS patients present with relapsing – remitting MS characterized by episodes of disability followed by recovery that eventually converts to a secondary progressive disease. Patients can also present with primary progressive disease (1–4).

Current approved therapies for MS target various mechanisms to modulate the immune system and limit disease. Interferon β activates the STAT transcription factors and modulates the immune system through multiple mechanisms including downregulating major histocompatibility complex (MHC) expression and blocking T cell migration (7). Glatiramer acetate has pleiotropic effects that include the induction of an anti-inflammatory T cell response (8). Teriflunomide inhibits dihydroorotate dehydrogenase, an enzyme involved in *de novo* nucleotide synthesis and the electron transport chain, and blocks lymphocyte proliferation (9). Modulators of the sphingosine-1-phosphate receptor including fingolimod, siponimod, ponesimod, and ozanimod limit lymphocyte egress from the lymph nodes (10). Cladribine incorporates into DNA, possibly inhibits the *de novo* nucleotide synthesis enzyme ribonucleotide reductase, and induces cell death in lymphocytes (11). Mitoxantrone intercalates into DNA and blocks T cell, B cell, and macrophage proliferation among other mechanisms (12). Methyl fumarates activate the transcription factor Nrf2 and

reduce lymphocyte levels (13). Natalizumab binds to α4β1 integrin and limits leukocyte egress from the blood vessels (14). Anti-CD52 antibodies (alemtuzumab) and anti-CD20 antibodies (ocrelizumab and ofatumumab) bind to CD52 on B and T lymphocytes and CD20 on B lymphocytes, respectively, leading to the depletion of these cell types (15,16). Although these therapies are effective, none of them completely blocks disease or disease progression, and all of them are associated with significant side effects that include liver injury, severe lymphopenia, and an increased risk of viral infections (17). Additional therapies to treat MS patients with single agent efficacies and low side-effect profiles are needed.

The deoxyribonucleoside salvage pathway consumes extracellular deoxyribonucleosides for the biosynthesis of deoxyribonucleoside triphosphates (dNTPs) to use in DNA synthesis and complements dNTP production from the *de novo* pathway (18). In the salvage pathway, deoxyribonucleosides are transported across the cell membrane by concentrative and equilibrative nucleoside transporters and are subsequently phosphorylated by deoxycytidine kinase (dCK), the rate-limiting enzyme in this pathway (18–21). dCK functions as a dimer in cells to phosphorylate deoxycytidine as its major substrate as well as deoxyadenosine and deoxyguanosine and can activate various nucleoside analogue therapeutics such as cytarabine and cladribine (22). The nucleoside analogue positron emission tomography (PET) radiotracers 1-(2'-deoxy-2'-[^{18}F]fluoroarabinofuranosyl)cytosine ([^{18}F]FAC) and 2-chloro-2′-deoxy-2′-[^{18}F]fluoro-9-β-D-arabinofuranosyl-adenine ([^{18}F]CFA) are acted upon by these same nucleoside transporters and by dCK and thus can visualize the deoxyribonucleoside salvage pathway and quantify deoxyribonucleoside salvage activity in mice and humans, respectively (23,24). The specificity of [^{18}F]FAC for deoxyribonucleoside salvage and dCK has been demonstrated using dCK knockout mice that fail to accumulate [^{18}F]FAC in any of the major organs in which [^{18}F]FAC normally accumulates such as the spleen and bone marrow (21). dCK is overexpressed at the mRNA level in tumor tissue from many different cancer types including esophageal carcinoma, cholangiocarcinoma, head and neck squamous cell carcinoma, hepatocellular carcinoma, and stomach adenocarcinoma and is likely involved in maintaining adequate dNTP pools during rapid cancer cell division (25,26). Additionally in cancer cells, dCK is activated in response to ionizing radiation and DNA damage through phosphorylation of Serine 74 by the ataxia telangiectasia mutated (ATM) and Ataxia telangiectasia and Rad3-related (ATR) enzymes where it contributes to DNA repair and the G2/M checkpoint (27–29).

In healthy mice and in humans, the deoxyribonucleoside salvage pathway is selectively enriched in lymphoid organs including the bone marrow, spleen, and lymph nodes (23,24). Mice lacking dCK have a defect in T and B cell development and splenomegaly possibly due to extramedullary hematopoiesis but are otherwise phenotypically normal with a normal life span (21). During T and B cell development, loss of dCK leads to depletion of intracellular deoxycytidine triphosphate pools, replication stress, and cell cycle arrest (30). Deoxyribonucleoside salvage activity is increased in T cells during activation in culture and in the spleen and lymph nodes in mouse models of systemic lupus erythematosus, autoimmune hepatitis, and inflammatory bowel disease and in a mouse model of anti-tumor immunity (23,31–33). In addition, we previously showed in the experimental autoimmune encephalomyelitis (EAE) model of MS that deoxyribonucleoside salvage activity is

increased in the lymph nodes and spleen at one time point in the disease (34). These data suggest a potential functional role for deoxyribonucleoside salvage in multiple autoimmune diseases including MS. Here we demonstrate that dCK is required for and can be targeted to block clinical symptoms in the EAE model of MS.

Methods:

Mice.

10-week-old, male and female C57BL/6N mice were used for experiments at the University of California, Los Angeles (UCLA). 10-week-old female C57BL/6N mice were used for experiments at Crown Biosciences. 7-week-old female C57BL/6J mice were used for experiments at Charles River Laboratories. All mice were purchased from Charles River Laboratories. All mouse studies at UCLA were approved of by the UCLA Animal Resource Committee. All mouse experiments at Crown Biosciences and Charles River Laboratories were per their established EAE protocols and complied with local animal welfare guidelines.

EAE induction.

Myelin oligodendrocyte glycoprotein peptide fragment 35 – 55 ($MOG_{35–55}$) model: Mice were acclimated to the animal facility for at least 7 days before starting the experiment. At UCLA, mice were injected subcutaneously at two sites on the back with an emulsion of $MOG_{35–55}$ peptide and Complete Freund's Adjuvant (CFA; 100 μL/injection; 100 μg $MOG_{35–55}$/injection; Hooke Laboratories EK-2110), and two hours and again 24 hours later, the mice were injected intraperitoneal with pertussis toxin (80 ng; 100 μL). At Crown Biosciences, mice were injected subcutaneously on each leg flank with an emulsion of $MOG_{35–55}$ peptide and CFA (100 μL/injection; 50 μg $MOG_{35–55}$/injection), and immediately after and again 48 hours later, the mice were injected intraperitoneally with pertussis toxin (200 ng; 100 μL). At Charles River Laboratories, mice were injected subcutaneously with an emulsion of $MOG_{35–55}$ peptide and CFA (100 μL/injection; 150 μg $MOG_{35–55}$/injection) at two sites on the lower back on Day 0 and two sites on the upper back on Day 7, and immediately after and again 48 hours after the first set of emulsion injections, mice were injected intraperitoneal with pertussis toxin (500 ng; 100 μL) (Table S1). *$MOG_{1–125}$ model:* EAE was induced in mice with the $MOG_{1–125}$ peptide following the same protocol as was used at UCLA for inducing EAE with the $MOG_{35–55}$ peptide except that an emulsion of $MOG_{1–125}$ peptide and CFA was used (80 μg $MOG_{1–125}$/injection; Hooke Laboratories EK-2160). All mice were scored following the standard clinical score that ranges from 0 to 5 where a score of 0 represents no phenotypes; a score of 1 represents a limp tail; a score of 2 represents a limp tail and hind leg weakness; a score of 3 represents a limp tail and complete hind leg paralysis; a score of 4 represents a limp tail, complete hind leg paralysis, and partial front leg paralysis; and a score of 5 represents complete limb paralysis or death.

[^{18}F]FAC PET/CT imaging.

[^{18}F]FAC PET/CT imaging was conducted as previously described (34). Briefly, mice were anesthetized with isoflurane, injected via the tail vein with ~1.4 MBq (40 μCi) of [^{18}F]FAC, and one hour later, imaged on the G8 or GNEXT PET/CT preclinical imaging system

(SOFIE). Results were analyzed by drawing regions of interest around the lymph nodes, spleen, bone marrow, spinal cord, and brain using the AMIDE medical imaging software. [^{18}F]FAC accumulation in each measured organ was quantified as percent injected dose per cubic centimeter except for in the PET images of the vehicle- and TRE-515-treated mice. To account for the higher background levels of [^{18}F]FAC in the TRE-515-treated mice, results were quantified as signal/background where background is muscle [^{18}F]FAC accumulation.

Ex vivo measurements of deoxyribonucleoside salvage activity.

Ex vivo measurements of deoxyribonucleoside salvage activity were conducted as previously described (34) except that cells were isolated from the lymph nodes and spleen.

TRE-515 treatments.

TRE-515 was dissolved to a concentration of 12.5 mg/mL in 40% captisol (w/v) vehicle. Mice were treated daily with TRE-515 via oral gavage at a dose and frequency of 75 mg/kg twice-a-day (BID), 100 mg/kg once-a-day (QD), and 150 mg/kg QD. Treatments were initiated at Day 1 post-EAE induction (UCLA and Crown Biosciences), at Day 11 post-EAE induction when all the mice had reached a clinical score of 1 or greater (UCLA), or at Day 7 post-EAE induction when a third of the mice had reached a clinical score of 0.5 (Charles River Laboratories).

Immunohistochemistry.

Immunohistochemistry was conducted as previously described except that spinal cord sections were analyzed (34). Spinal cord sections were stained with Luxol fast blue by incubating the tissue in Luxol fast blue solution overnight at 65°C, differentiating the tissue with lithium carbonate solution, and counterstaining the tissue using cresyl violet solution per the manufacturer's protocol (IHC World).

Plasma deoxycytidine levels.

EAE mice (14 days post-EAE induction) were treated with vehicle or TRE-515 (75 mg/kg) and blood was collected at 4 hours post-treatment. Plasma deoxycytidine levels were analyzed as previously described (24).

TRE-515 pharmacokinetic studies.

Naïve and EAE mice (14 days post-EAE induction when all the mice had reached a clinical score > 2.5) were treated with vehicle or TRE-515 (75 mg/kg). 1, 4, and 12 hours post-treatment, the brain, spinal cord, and blood were collected, and TRE-515 levels in these tissues were analyzed similar to previously described (35).

Tetramer studies.

An allophycocyanin (APC)-labeled $MOG_{38–49}$ I-A(b) tetramer and control I-A(b) tetramer were obtained from the NIH Tetramer Core Facility at Emory University. $MOG_{35–55}$ EAE mice were treated with vehicle or TRE-515 (150 mg/kg, QD) starting on Day 1 post-EAE induction. On Day 10 post-EAE induction, cells from the inguinal, axial, and cervical lymph nodes were isolated by grinding the tissue between two glass slides

in RPMI-1640 media containing 10% (v/v) fetal bovine serum, glutamine (2 mM), and penicillin-streptomycin (100 U/mL). Cells were left unstained or were stained with either an APC-labeled $MOG_{38–49}$ I-A(b) tetramer or control I-A(b) tetramer (NIH Tetramer Core Facility, Emory University; 18 μg/mL; 37 °C; 30 min) followed by a phycoerythrin (PE)-labeled anti-mouse CD4 antibody (eBioscience 12–0042-81; 1.25 μg/mL; 4 °C; 30 min) and 4′,6-diamidino-2-phenylindole (DAPI; 1.2 μM). Cells were gated for single, live, $CD4^+$ cells, and the percent tetramer positive cells for each sample was quantified.

CyTOF.

$MOG_{35–55}$ EAE mice were treated daily with vehicle or TRE-515 (150 mg/kg, QD) starting on Day 1 post-EAE induction. On Day 3 and Day 10 post-EAE induction, cells from the lymph nodes and spleens of the EAE mice were isolated as described above. Red blood cells in the spleen were lysed using ammonium-chloride-potassium (ACK) lysis buffer. Cells were immunostained and analyzed by CyTOF with the antibodies in Table 1 as previously described (36) except that following the surface staining, cells were stained with the intracellular markers by fixing the cells with paraformaldehyde (2%, 10 min, room temperature), washing the cells twice with Perm-S buffer (2 mL; Fluidigm 201066), adding the intracellular markers in Perm-S buffer (1 hour, room temperature), and washing the cells twice with Maxpar Cell Staining Buffer (2 mL; Fluidigm 201068). Data was analyzed using the OMIQ software. Cells were gated for live, single, $CD45^+$ cells and subsampled so that each sample had equal numbers of cells. Cells from each time point and organ system were analyzed separately using the FlowSOM algorithm, which creates self-organizing maps by clustering cells into nodes and further organizing the nodes by consensus metaclustering into 20 non-overlapping metaclusters. The Significance Analysis of Microarrays (SAM) software (number of permutations: 500; false discovery rate cutoff: 0.1) was used to identify metaclusters for which the percent of cells in that metacluster differed significantly with TRE-515 treatments. The SAM software occasionally identified metaclusters with high variance and small differences between vehicle- and TRE-515-treated samples. To focus on the most significantly different clusters, we conducted T tests on each metacluster identified by SAM as significant, and only further analyzed those with $p<0.1$. Median marker expression for a given marker represents the median expression of that marker across all samples.

Blood cell counts.

Blood (100 μL) was collected via a retroorbital bleed into K_2-EDTA tubes from $MOG_{35–55}$ EAE mice Day 28 post-EAE induction following daily treatment with vehicle or TRE-515 (100 mg/kg, QD) starting on Day 1 post-EAE induction and was analyzed by a Vetscan hematology analyzer to quantify white blood cells, lymphocytes, neutrophils, monocytes, red blood cells, and platelet cells.

Statistical analyses.

Statistical significance was determined by unpaired T-tests, and one-way and two-way ANOVA analyses with Dunnett and Tukey multiple comparison corrections. CyTOF data was analyzed by SAM.

Results:

Deoxyribonucleoside salvage activity is elevated in T cells in the lymph nodes of EAE mice

EAE is the standard mouse model for studying the biology of and testing new therapies for MS. This mouse model can be induced by injecting C57BL/6 mice with an emulsion containing amino acids 35 – 55 of the mouse MOG protein ($MOG_{35–55}$) and CFA followed by two injections with pertussis toxin (37). $MOG_{35–55}$ EAE develops in mice lacking B cells but requires T cells and is considered a B-cell independent model (38). Following injection of the $MOG_{35–55}$/CFA emulsion, mice remain asymptomatic for approximately 10 days, after which they manifest clinical phenotypes starting with a limp tail and leading to hind limb and forelimb paralysis that peak approximately 4 days later. The severity of clinical phenotypes is quantified on a scale of 0 to 5.

We have previously shown that the deoxyribonucleoside salvage pathway is activated in the lymph nodes and spleen of $MOG_{35–55}$ EAE mice at Day 14 post-EAE induction during which the mice were at peak disease (34). However, whether deoxyribonucleoside salvage is activated in these tissues at other stages of the disease remained to be determined. The deoxycytidine analogue PET radiotracer [^{18}F]FAC can be used to quantify deoxyribonucleoside salvage activity non-invasively in tissues throughout the body and allows us to study this pathway without perturbation in its natural *in vivo* environment. To investigate at which EAE disease stages immune cells activate deoxyribonucleoside salvage, we induced EAE in female and male mice with the $MOG_{35–55}$ peptide/CFA emulsion and imaged the mice with [^{18}F]FAC PET/CT pre-induction and at 7, 14, 21, and 28 days post-EAE induction. These time points represent different stages of disease in this model including the pre-symptomatic stage (Day 7 post-EAE induction), peak disease (Days 14 and 21 post-EAE induction), and mild remission (Day 28 post-EAE induction). [^{18}F]FAC accumulation was quantified in the lymph nodes, spleen, spinal cord, and brain. [^{18}F]FAC accumulation was elevated in the spleen and lymph nodes of both the female and male mice starting as early as 7 days post-EAE induction and remained elevated through Day 28 post-EAE induction relative to pre-induction mice (Fig. 1a, b; Fig. S1). This suggests that immune cells in the secondary lymphoid organs activate and potentially rely on the deoxyribonucleoside salvage pathway throughout the EAE disease. Additionally, [^{18}F]FAC accumulation was elevated in the brains of female and male $MOG_{35–55}$ EAE mice at Days 7 and 14 post-EAE induction and throughout disease, respectively, relative to pre-induction mice, likely due to brain-infiltrating leukocytes in these mice (34) and was elevated in the spinal cords of male but not female $MOG_{35–55}$ EAE mice (Fig. S1, S2).

Higher [^{18}F]FAC accumulation in the spleen and lymph nodes of $MOG_{35–55}$ EAE mice likely represents both a change in the cellular composition of these organs during disease and an increase in deoxyribonucleoside salvage activity in specific cell types residing in those organs. To quantify changes in deoxyribonucleoside salvage activity in specific cell types at different disease stages, we isolated CD11b innate immune cells, CD4 T cells, CD8 T cells, and CD45R (B220) B cells from the lymph nodes and spleens of $MOG_{35–55}$ EAE mice early (Days 7 – 14 post-EAE induction) or late (Days 21 – 28 post-EAE induction) in the disease course and measured deoxyribonucleoside salvage activity with

[^{3}H]deoxycytidine. In cells from the lymph nodes, deoxyribonucleoside salvage activity was elevated in CD4 and CD8 T cells early in the disease course but returned to pre-induction levels at the later time point. Deoxyribonucleoside salvage activity was unaffected in the innate immune (all types) or B cells of the lymph nodes at any time point in the disease course (Fig. 1c). In the spleen, deoxyribonucleoside salvage activity was significantly elevated in CD11b innate immune cells during late disease (Fig. S3). Deoxyribonucleoside salvage activity remained unaffected in the CD4 and CD8 T cells and B cells in the spleen at any point in the disease. Collectively, these results suggest that T lymphocytes in the lymph nodes activate deoxyribonucleoside salvage activity during immune activation in the $MOG_{35–55}$ EAE mouse model.

TRE-515 blocks deoxyribonucleoside salvage activity in the lymphoid organs

Our data demonstrating that CD4 and CD8 T cells increase deoxyribonucleoside salvage activity during periods of immune activation in $MOG_{35–55}$ EAE mice suggests a potential functional role for this pathway in the development of clinical symptoms in EAE. TRE-515 is a recently developed small molecule inhibitor of dCK, the rate-limiting enzyme in the deoxyribonucleoside salvage pathway, and analogues of TRE-515 have been shown to block deoxyribonucleoside salvage in xenograft tumors (39,40). To evaluate whether TRE-515 blocks deoxyribonucleoside salvage activity in the lymphoid organs, we treated mice with vehicle or TRE-515 (150 mg/kg) once and imaged the mice with [^{18}F]FAC PET/CT. TRE-515 blocked [^{18}F]FAC accumulation in the bone marrow and spleen (Fig. 2a, b) while the percent of major immune cell populations in these organs remained unaltered following this acute dosing (Fig. 2c). The lymph nodes of these mice proved too small to accurately quantify a decrease in [^{18}F]FAC accumulation following TRE-515 treatment. TRE-515 at a dose of 75 mg/kg also blocked deoxyribonucleoside salvage activity and increased plasma deoxycytidine levels (Fig. S4a – c), an expected result given that dCK is required for the cellular consumption of deoxycytidine from the plasma. In both the 75 mg/kg and 150 mg/kg TRE-515-treated mice, TRE-515 blocked [^{18}F]FAC accumulation to a greater extent in the bone marrow than the spleen. This could be due to greater concentrations of TRE-515 reaching the bone marrow than the spleen or other explanations.

TRE-515 limits clinical symptoms in EAE mice

The ability of TRE-515 to target dCK and block deoxyribonucleoside salvage activity in the lymphoid organs of mice allowed us to test whether dCK and the deoxyribonucleoside salvage pathway contributes to and can be targeted to limit clinical phenotypes in EAE mice at different stages of disease. To evaluate whether targeting dCK prophylactically at disease induction could limit disease phenotypes, we induced $MOG_{35–55}$ EAE in mice and treated the mice with vehicle or TRE-515 (150 mg/kg QD) starting the next day and through Day 21 post-EAE induction. The EAE mice treated with TRE-515 developed symptoms later, had fewer symptoms at peak disease, and had fewer symptoms overall compared to EAE mice treated with vehicle (Fig. 3a – c). TRE-515 also limited clinical symptoms in the $MOG_{35–55}$ EAE model at once daily dosing of 100 mg/kg, at twice daily dosing of 75 mg/kg, and whether the EAE was induced in male or female mice (Fig. S4d – f). Clinical symptoms in the EAE model occur secondary to demyelination caused by infiltrating leukocytes in the

CNS (37). TRE-515-treated $MOG_{35–55}$ EAE mice have fewer infiltrating leukocytes in the CNS and less demyelination compared with vehicle-treated EAE mice (Fig. 3d).

EAE induced with the $MOG_{35–55}$ peptide is the best-studied EAE model but in contrast to MS is B-cell independent (38). In contrast, EAE induced with amino acids 1 – 125 of the mouse MOG protein ($MOG_{1–125}$ peptide) fails to manifest in mice lacking B cells and thus is considered a B cell-dependent disease (38). Though less studied, this model allows us to investigate the deoxyribonucleoside salvage pathway and the effects of TRE-515 in a mouse model that more accurately models the B cell involvement of MS. $MOG_{1–125}$ EAE mice present with disease following a similar time course as the $MOG_{35–55}$ EAE model. We imaged $MOG_{1–125}$ EAE mice with [^{18}F]FAC PET/CT pre-induction and at Day 14 post-EAE induction when the mice had reached peak disease. Similar to the $MOG_{35–55}$ EAE mice, $MOG_{1–125}$ EAE mice had significantly higher [^{18}F]FAC accumulation in the lymph nodes compared to pre-induction mice, suggesting activation of the deoxyribonucleoside salvage pathway in this tissue (Fig. 4a, b). $MOG_{1–125}$ EAE mice also had significantly elevated [^{18}F]FAC accumulation in the brain compared to pre-induction mice, likely due to [^{18}F]FAC accumulation in brain-infiltration leukocytes (34). We treated $MOG_{1–125}$ EAE mice with TRE-515 starting on Day 1 post-EAE induction. TRE-515 limited clinical symptoms in the $MOG_{1–125}$ EAE model at once daily dosing of 150 mg/kg but not twice daily dosing of 75 mg/kg (Fig. 4c, d). These data indicate that deoxyribonucleoside salvage is upregulated in immune cells during immune activation and that TRE-515 can limit clinical symptoms in EAE models driven by just T cells or by both T and B cells.

To evaluate whether targeting dCK therapeutically could limit disease progression, $MOG_{35–55}$ EAE mice were treated with vehicle or TRE-515 (150 mg/kg QD) starting when the mean clinical score for the mice reached 1, which in this experiment occurred on Day 11. Within five days of starting treatments, EAE mice treated with TRE-515 began to have significantly fewer clinical symptoms than vehicle-treated EAE mice, and this was maintained for the remainder of the treatment period, yielding fewer EAE symptoms overall (Fig. 5a, b). Similar to the mice treated starting on Day 1 post-EAE induction, the mice treated starting on Day 11 post-EAE induction had fewer infiltrating leukocytes in the CNS and less CNS demyelination (Fig. 5c).

Evaluating clinical symptoms in EAE models is necessarily subjective and could be affected by observer bias. Additionally, the development of symptoms in this model can be affected by various difficult to account for variables including stress (41). To evaluate the rigor and reproducibility of these experiments and to further validate and expand on these results, we tested the efficacy of TRE-515 in established EAE protocols at the Crown Biosciences and Charles River Laboratories contract research organizations. Consistent with the results of our earlier experiment (Fig. S4f), $MOG_{35–55}$ EAE mice treated at Crown Biosciences with TRE-515 (100 mg/kg QD) starting Day 1 post-EAE induction had fewer symptoms at peak disease, had fewer symptoms overall, and developed symptoms later compared with vehicle-treated EAE mice (Fig. S5a – c). In their established EAE protocol, the Charles River Laboratories contract research organization injects their mice with $MOG_{35–55}$ peptide/CFA emulsion at Day 0 and again at Day 7 to yield a disease with monotonically increasing symptoms without remission. Similar to the results of our earlier experiment (Fig. 5a, b),

$MOG_{35–55}$ EAE mice treated at Charles River Laboratories with vehicle or TRE-515 (75 mg/kg BID) starting on Day 7 post-EAE induction (when at least a third of the mice showed symptoms) had fewer symptoms than vehicle-treated $MOG_{35–55}$ EAE mice (Fig. S5d, e). Additionally, half of the $MOG_{35–55}$ EAE mice treated with TRE-515 at Charles River Laboratories began to recover from their symptoms starting at Day 20 post-EAE induction and a third of those mice recovered from all symptoms and returned to a clinical score of 0. The TRE-515-treated EAE mice that showed recovery in this model had fewer infiltrating leukocytes in the CNS and less demyelination than the vehicle-treated EAE mice (Fig. S5f).

Collectively, our data strongly demonstrate that targeting dCK with the small molecule inhibitor TRE-515 can limit clinical symptoms in the EAE mouse model when treatments are started either at disease induction or when symptoms arise.

TRE-515 blocks CD4 T and B cell activation-induced proliferation in the EAE mouse model

Our data demonstrates that TRE-515 can block symptoms in EAE mice. TRE-515 could be having this effect by directly affecting cells in the CNS or in the periphery. To test whether TRE-515 can cross the blood-brain and blood-spinal cord barrier, we treated naïve and $MOG_{35–55}$ EAE mice with TRE-515 and measured TRE-515 levels in the plasma, brain, and spinal cord of these mice 1, 4, and 12 hours later. TRE-515 levels in the brain and spinal cord were less than 4% and 7% of TRE-515 levels in the plasma, respectively, independent of whether the mice were induced with EAE (Fig. S6). These results combined with our earlier data showing that mice treated with TRE-515 have fewer infiltrating leukocyte in the CNS (Fig. 3d, 5c) argue against the possibility that TRE-515 directly affects cells in the CNS to modulate EAE phenotypes and instead focused our attention on how TRE-515 affects immune cells in the periphery.

In $MOG_{35–55}$ EAE mice, CD4 T cells that express a T cell receptor that recognizes the $MOG_{35–55}$ peptide (MOG-specific CD4 T cells) are primary drivers of disease (42,43). Blocking these myelin-specific CD4 T cells could be one way in which TRE-515 limits clinical symptoms in this model. We quantified these cells using a fluorescently labeled tetramer that presents a peptide consisting of amino acids 38 – 49 of the mouse MOG protein ($MOG_{38–49}$) on a Class II MHC protein. As a negative control, we used a fluorescently labeled tetramer that presents a peptide not targeted by a mouse CD4 T cell. $MOG_{35–55}$ EAE induction caused a significant expansion of the MOG-specific CD4 T cells compared to naïve mice that was blocked by TRE-515 treatment (Fig. 6a). The percent of CD4 T cells that bound to the control tetramer was not significantly affected by the EAE induction or the TRE-515 treatment (Fig. 6a) indicating that our results with the $MOG_{38–49}$ peptide-expressing tetramer were specific. These data suggest that TRE-515 blocks the expansion of MOG-specific CD4 T cells.

In addition to blocking the expansion of MOG-specific CD4 T cells, TRE-515 could affect other cells of the immune system in the $MOG_{35–55}$ EAE model to limit clinical symptoms or alternatively in a way that would be predicted to yield significant side effects from the treatment. To comprehensively analyze the immune system in these experiments, we used mass cytometry (CyTOF) to profile the immune system at Day 3 and Day 10 post-EAE induction in the spleen and lymph nodes of $MOG_{35–55}$ EAE mice treated with vehicle or

TRE-515 (150 mg/kg QD) starting on Day 1 post-EAE induction. Results were analyzed by FlowSOM, an algorithm that performs unsupervised clustering of the cells to create maps with nodes representing different cell types and states, which the algorithm then organizes into metaclusters. The statistical method SAM was used to identify metaclusters for which the percent of cells in that metacluster is significantly related to the TRE-515 treatment relative to the vehicle treatment (44,45).

In each organ and at each time point, the FlowSOM algorithm clustered the cells into major immune cell classes including CD4 T cells, CD8 T cells, B cells, and innate immune cells (Fig. S7). In the lymph nodes on Day 3 post-EAE induction, TRE-515 significantly decreased the percent of cells in two metaclusters representing activated and proliferating CD4 T cells (CD4 T cell Metaclusters 11 and 12 with elevated levels of CD69, CD39, CD44, and Ki67 and low levels of CD62L compared to the naïve CD4 T cell Metacluster 16) and two B cell metaclusters representing proliferating plasmablasts (B cell Metacluster 17 and 18 with elevated levels of CD69, CD138, and Ki67 compared to naïve B cell Metacluster 1) (Fig. 6b – d; Table S2). TRE-515 had no significant effect on the percent of cells in any other metacluster including the naïve CD4 T cell metacluster, an activated but non-dividing CD4 T cell metacluster (CD4 T cell Metacluster 15 with elevated levels of CD69 and CD39 and low levels of Ki67 compared to the naïve T cell Metacluster 16), the naïve B cell metacluster, any CD8 T cell metacluster, and any $CD11b^+$ innate immune cell metacluster (Table S2). In the spleen on Day 3 post-EAE induction, TRE-515 significantly decreased the percent of cells in a proliferating plasmablast metacluster (B cell Metacluster 14 with elevated levels of CD69, CD138, and Ki67 compared to naïve B cell Metacluster 3) but had no effect on any of the other metaclusters including the naïve B cell metacluster or any of the innate immune metaclusters (Fig. 6e, f; Table S3). These data suggest that TRE-515 blocks activation-induced proliferation in CD4 T cells and B cells in our model without affecting the levels of naïve CD4 T cells, naïve B cells, CD8 T cells, or innate immune cells.

In the lymph nodes from Day 10 post-EAE induction, TRE-515 significantly increased the percent of cells in the metacluster representing naïve T cell (CD4 T cell Metacluster 18 with high levels of CD62L and low levels of CD69, CD39, CD44, and Ki67) while decreasing the percent of cells in the metacluster representing activated T cell (CD4 T cell Metacluster 8 with low levels of CD62L and elevated levels of CD69, CD39, CD44, and Ki67 compared to the naïve CD4 T cell Metacluster 18) (Fig. 7a, b; Table S4). TRE-515 had no effect on other CD4 T cell metaclusters or metaclusters representing B and CD8 T cells (Table S4). In the spleen from Day 10 post-EAE induction, TRE-515 decreased the percent of cells in a metacluster representing memory T cells (CD4 T cell Metacluster 10 with low levels of CD62L, CD69, and Ki67 and high levels of CD44 compared to naïve CD4 T cell Metacluster 7) but did not significantly affect the percent of cells in any other metacluster including the naïve CD4 T cell metacluster (Fig. 7c, d; Table S5).

In total, our tetramer and CyTOF data suggest that TRE-515 blocks B and CD4 T cell activation-induced proliferation early in the $MOG_{35–55}$ EAE disease course, leading to more naïve T cells and fewer memory T cells than in vehicle-treated $MOG_{35–55}$ EAE mice without decreasing the levels of other major immune cell types including naïve CD4 or

CD8 T cells, naïve B cells, or CD11b innate immune cells. These results are consistent with cell counts from the blood of EAE mice treated with vehicle or TRE-515 for 28 days (Fig. S5) that show minimal to no effect of TRE-515 on the levels of total white blood cells, lymphocytes, neutrophils, monocytes, platelets, and red blood cells (Fig. S8).

Discussion:

Here we show that the dCK inhibitor TRE-515 limits the development of clinical symptoms and blocks CD4 T and B cell activation-induced proliferation in the $MOG_{35–55}$ EAE mouse model. Activated CD4 T cells are key drivers of pathology in the $MOG_{35–55}$ EAE model (42,43), and TRE-515 blocks the proliferation of activated CD4 T cells in this model at both Day 3 and Day 10 post-EAE induction. These data strongly suggest that TRE-515 abrogates clinical symptoms in this model by blocking activation-induced proliferation of CD4 T cells. Additionally, by Day 10 post-EAE induction, mice treated with TRE-515 have fewer memory CD4 T cells, an expected result of blocking CD4 T cell activation-induced proliferation. B cells likely do not contribute to clinical phenotypes in the $MOG_{35–55}$ EAE model (38). However, we also show that TRE-515 has efficacy in the $MOG_{1–125}$ EAE model in which B cells contribute to disease. TRE-515 may be limiting clinical symptoms in this model through its effect on both T and B cells.

We evaluated the effect of TRE-515 on clinical symptoms in multiple experiments using different sexes (male and female), treatment paradigms (prophylactic or therapeutic), TRE-515 doses (75 mg/kg BID, 100 mg/kg QD, and 150 mg/kg QD), and EAE models ($MOG_{35–55}$ and $MOG_{1–125}$). Efficacy can be evaluated as the percent decrease in the mean clinical score of the drug-treated mice when the vehicle-treated mice reach peak disease and compared across experiments. In those experiments in which we used the same sex, treatment paradigm, and EAE model, the efficacy of TRE-515 across experiments was similar. In all four of the experiments in which we prophylactically treated female $MOG_{35–55}$ EAE mice with TRE-515 (Fig. 3a; Fig. S4d, S4f, S5a), TRE-515 had an efficacy of 29%, 36%, 45%, and 45%. In the two experiments in which we therapeutically treated female $MOG_{35–55}$ EAE mice with TRE-515 (Fig. 5a; Fig. S5d), TRE-515 had an efficacy of 34% and 44% although with some notable differences in the kinetics of the response. Within these experiments, we did not identify a clear dose response for TRE-515 although the dose range was limited and it could be that nearly equivalent target inhibition occurs across this range of doses. We do identify notable differences in the efficacy of TRE-515 when we compare across different sexes and models. At the 75 mg/kg dose, prophylactic TRE-515 treatments of $MOG_{35–55}$ EAE mice had an efficacy of 45% in female mice but 62% in male mice (Fig. S4d, S4e). At the 75 mg/kg dose, prophylactic TRE-515 treatments had an efficacy of 45% in female $MOG_{35–55}$ EAE mice but by a non-statistically significant 9% in female $MOG_{1–125}$ EAE mice (Fig. 4d; Fig. S4d). We cannot readily explain the differences we see between female and male mice. We speculate that higher doses of TRE-515 may be required to limit the proliferation of both the T and B cells that drive disease in the $MOG_{1–125}$ model compared with just the T cells that drive disease in the $MOG_{35–55}$ model (38).

Cells use two major pathways to synthesize dNTPs for DNA synthesis: the *de novo* nucleotide synthesis pathway and the deoxyribonucleoside salvage pathway (18). In the *de novo* nucleotide synthesis pathway, dNTPs are synthesized from consumed glucose and amino acids through a stepwise process. In the deoxyribonucleoside salvage pathway, complete deoxyribonucleosides are consumed from extracellular space and phosphorylated to dNTPs. Here we show that the proliferation of B and CD4 T cells in the lymph nodes and B cells in the spleen at Day 3 post-EAE induction can be blocked by inhibiting dCK, suggesting that these cells require deoxyribonucleoside salvage for their proliferation under these conditions. At the same time, we did not identify any innate immune cell types that are affected by dCK inhibition, even though a number of innate immune cell metaclusters have similar Ki67 levels as the proliferating B and CD4 T cell metaclusters. Similarly, lifetime dCK knockout mice develop normally except for a defect in lymphocyte development (21). These data suggest that innate immune cells and cells other than lymphocytes that divide during development do not require deoxyribonucleoside salvage. Why certain cell types require both deoxyribonucleoside salvage and the *de novo* nucleotide synthesis pathway while other cell types require only the *de novo* nucleotide synthesis pathway for deoxyribonucleotide synthesis remains unclear. However, studies show that thymidine can block the synthesis of deoxycytidine triphosphate in the *de novo* pathway via inhibition of the rate-limiting enzyme ribonucleotide reductase (30). High thymidine levels in the bone marrow and thymus of adolescent mice relative to other tissues likely shifts developing T and B cells to using the salvage pathway to maintain adequate deoxycytidine triphosphate levels (30). We speculate that the same may be true for T and B cells activated in the lymph nodes of adult mice. Notably, at least in adolescent mice, thymidine levels in the lymph nodes are similar to thymidine levels in the thymus and bone marrow (30).

It remains to be determined how blocking dCK limits B and CD4 T cell activation-induced proliferation in the $MOG_{35–55}$ EAE mouse model. However, lack of dCK in rapidly proliferating Hardy fraction B-C B cell progenitors, DN3b T cell precursors, and nucleated erythroblast erythrocyte precursors yields lower levels of deoxycytidine triphosphates and promotes replication stress, cell cycle arrest at early S phase, and blocked proliferation (30). One hypothesis is that these same mechanisms are present in mature, naïve B and T cells and are activated in response to dCK inhibition during activation-induced proliferation of B and T cells. We do not identify a change in the total number of red blood cells in mice treated for up to 28 days with TRE-515 suggesting that deoxyribonucleoside salvage does not contribute significantly to maintaining erythrocyte levels after development. Testing this and other hypotheses will be the subject of future studies.

Most approved MS therapies have been tested in $MOG_{35–55}$ EAE mice, which allows us to compare the preclinical efficacy of TRE-515 to approved therapies in this model. Efficacy can be evaluated as described above and compared across treatments. When treatments are started at disease induction, TRE-515 has a median efficacy of 45% compared to leflunomide (a metabolic precursor of teriflunomide) with a median efficacy of ~25%, Interferon β with a median efficacy of ~40%, dimethyl fumarate with a median efficacy of ~40%, glatiramer acetate with a median efficacy of ~65%, and fingolimod with a median efficacy of ~70% (46–64). When treatments are started at symptom onset, TRE-515 has a median efficacy of 39% compared to Interferon β with a median efficacy of 0%,

teriflunomide with a median efficacy of 0%, dimethyl fumarate with a median efficacy of ~35%, fingolimod with a median efficacy of ~35%, and glatiramer acetate with a median efficacy of ~65% (46–50,65–69). The efficacy of a therapy in patients with MS will be surely different than the efficacy of that therapy in the $MOG_{35–55}$ EAE model for many reasons including differences in underlying biology and the achievable dose of a therapy in patients. Nevertheless, these and our studies provide early data to suggest that TRE-515 is similarly efficacious in the $MOG_{35–55}$ EAE model to other approved therapies that have reached the clinic and have a measurable impact of MS patients.

Enzymes in nucleotide synthesis pathways are effective targets for limiting clinical symptoms both in the $MOG_{35–55}$ EAE mouse model as well as in patients with MS although to date all nucleotide synthesis inhibitors have targeted the *de novo* nucleotide synthesis pathway. The clinical inhibitor teriflunomide inhibits dihydroorotate dehydrogenase, an enzyme in the *de novo* pyrimidine biosynthesis pathway that converts dihydroorotate to orotate (9). The clinical inhibitor cladribine is a prodrug that accumulates in cells and is phosphorylated to cladribine diphosphate and cladribine triphosphate. Cladribine likely has multiple mechanisms-of-action but one proposed mechanism includes reversible inhibition of ribonucleotide reductase by cladribine diphosphate and triphosphate (11). Ribonucleotide reductase catalyzes the reduction of ribonucleotide diphosphates to deoxyribonucleotide diphosphates (18). How targeting enzymes in the *de novo* nucleotide synthesis pathway will compare to targeting dCK in the deoxyribonucleoside salvage pathway with respect to both efficacy and side effect profiles in MS patients will only be determined in clinical trials. However, [^{18}F]CFA PET imaging of human subjects demonstrates that deoxyribonucleoside salvage activity is largely concentrated in the lymphoid organs in humans (24), suggesting that on-target side effects in patients – if any exist – may be limited to effects on the immune system.

Conclusions:

Here we show that pharmacological inhibition of dCK can block B and CD4 T cell activation-induced proliferation and limit symptoms in a mouse model of the autoimmune disease MS without decreasing the levels of other immune cell populations including naïve T and B cells and innate immune cells. In doing so, we define a potential new target for treating patients and modulating symptoms in MS. Most proteins and pathways that prove to be effective targets for immunomodulation in one autoimmune disease are subsequently shown to be effective targets in additional autoimmune diseases. B and T cells are also important contributors to many different autoimmune diseases including systemic lupus erythematosus and inflammatory bowel disease (70,71). Although it remains to be formally tested, based on the proposed mechanism-of-action of TRE-515 in the EAE model, we would hypothesize that TRE-515 may have efficacy across a wide range of autoimmune diseases and could represent a new type of immunomodulatory drug.

Supplementary Material

Refer to Web version on PubMed Central for supplementary material.

Acknowledgements:

We thank the Crump Institute Molecular Imaging Technology Center, the Crump Cyclotron and Radiochemistry Technology Center, the UCLA Translational Pathology Core Laboratory, and the NIH Tetramer Core Facility. CyTOF and flow cytometry experiments were conducted at the UCLA Jonsson Comprehensive Cancer Center (JCCC) and Center for AIDS Research Flow Cytometry Core Facility. We thank Dr. Oluwatayo Ikotun, Dr. Chiara Ghezzi, and Felix Bergara for technical assistance. This work was funded by NIH grants P30 CA016042, 5P30 AI028697, R21 AI119916, and R01 NS112287; the UCLA JCCC; the UCLA AIDS Institute; the David Geffen School of Medicine at UCLA; the UCLA Chancellor's Office; the UCLA Vice Chancellor's Office of Research; the UCLA Eugene Cota Robles Fellowship; the UCLA Brain Research Institute Knaub Fellowship for Multiple Sclerosis Research; and the Broad Stem Cell Research Center at UCLA.

Funding statement:

This work was funded by NIH grants P30 CA016042, 5P30 AI028697, R21 AI119916, and R01 NS112287; the UCLA JCCC; the UCLA AIDS Institute; the David Geffen School of Medicine at UCLA; the UCLA Chancellor's Office; the UCLA Vice Chancellor's Office of Research; the UCLA Eugene Cota Robles Fellowship; the UCLA Brain Research Institute Knaub Fellowship for Multiple Sclerosis Research; and the Broad Stem Cell Research Center at UCLA.

Data availability statement:

All data used in this study are included in the main article and supporting information.

Glossary:

MS	multiple sclerosis
dCK	deoxycytidine kinase
EAE	experimental autoimmune encephalomyelitis
CyTOF	mass cytometry
CNS	central nervous system
MHC	major histocompatibility complex
dNTPs	deoxyribonucleoside triphosphates
PET	positron emission tomography
[^{18}F]FAC	1-(2'-deoxy-2'-[^{18}F]fluoroarabinofuranosyl)cytosine
[^{18}F]CFA	2-chloro-2′-deoxy-2′-[^{18}F]fluoro-9-β-D-arabinofuranosyl-adenine
ATM	ataxia telangiectasia mutated
ATR	Ataxia telangiectasia and Rad3-related
UCLA	University of California, Los Angeles
$MOG_{35–55}$	Myelin oligodendrocyte glycoprotein peptide fragment 35 – 55
CFA	Complete Freund's Adjuvant
BID	twice-a-day

QD	once-a-day
APC	allophycocyanin
PE	phycoerythrin
DAPI	4′,6-diamidino-2-phenylindole
ACK	ammonium-chloride-potassium
SAM	Significance Analysis of Microarrays

References:

1. Thompson AJ, Baranzini SE, Geurts J, Hemmer B, Ciccarelli O. Multiple sclerosis. The Lancet. 2018 Apr;391(10130):1622–36.
2. Baecher-Allan C, Kaskow BJ, Weiner HL. Multiple Sclerosis: Mechanisms and Immunotherapy. Neuron. 2018 Feb 21;97(4):742–68. [PubMed: 29470968]
3. Reich DS, Lucchinetti CF, Calabresi PA. Multiple Sclerosis. N Engl J Med. 2018 Jan 11;378(2):169–80. [PubMed: 29320652]
4. Filippi M, Bar-Or A, Piehl F, Preziosa P, Solari A, Vukusic S, et al. Multiple sclerosis. Nat Rev Dis Primer. 2018 Nov 8;4(1):43.
5. Dendrou CA, Fugger L, Friese MA. Immunopathology of multiple sclerosis. Nat Rev Immunol. 2015 Sep 15;15(9):545–58. [PubMed: 26250739]
6. Li R, Patterson KR, Bar-Or A. Reassessing B cell contributions in multiple sclerosis. Nat Immunol. 2018 Jul;19(7):696–707. [PubMed: 29925992]
7. Jakimovski D, Kolb C, Ramanathan M, Zivadinov R, Weinstock-Guttman B. Interferon β for Multiple Sclerosis. Cold Spring Harb Perspect Med. 2018 Nov 1;8(11):a032003.
8. Aharoni R. The mechanism of action of glatiramer acetate in multiple sclerosis and beyond. Autoimmun Rev. 2013 Mar;12(5):543–53. [PubMed: 23051633]
9. Bar-Or A, Pachner A, Menguy-Vacheron F, Kaplan J, Wiendl H. Teriflunomide and its mechanism of action in multiple sclerosis. Drugs. 2014 Apr;74(6):659–74. [PubMed: 24740824]
10. McGinley MP, Cohen JA. Sphingosine 1-phosphate receptor modulators in multiple sclerosis and other conditions. Lancet Lond Engl. 2021 Sep 25;398(10306):1184–94.
11. Leist TP, Weissert R. Cladribine: mode of action and implications for treatment of multiple sclerosis. Clin Neuropharmacol. 2011 Feb;34(1):28–35. [PubMed: 21242742]
12. Fox EJ. Mechanism of action of mitoxantrone. Neurology. 2004 Dec 28;63(12 Suppl 6):S15–18. [PubMed: 15623664]
13. Mills EA, Ogrodnik MA, Plave A, Mao-Draayer Y. Emerging Understanding of the Mechanism of Action for Dimethyl Fumarate in the Treatment of Multiple Sclerosis. Front Neurol. 2018;9:5. [PubMed: 29410647]
14. Steinman L. The discovery of natalizumab, a potent therapeutic for multiple sclerosis. J Cell Biol. 2012 Oct 29;199(3):413–6. [PubMed: 23109666]
15. Hu Y, Turner MJ, Shields J, Gale MS, Hutto E, Roberts BL, et al. Investigation of the mechanism of action of alemtuzumab in a human CD52 transgenic mouse model. Immunology. 2009 Oct;128(2):260–70. [PubMed: 19740383]
16. Lee DSW, Rojas OL, Gommerman JL. B cell depletion therapies in autoimmune disease: advances and mechanistic insights. Nat Rev Drug Discov. 2021 Mar;20(3):179–99. [PubMed: 33324003]
17. Tintore M, Vidal-Jordana A, Sastre-Garriga J. Treatment of multiple sclerosis - success from bench to bedside. Nat Rev Neurol. 2019 Jan;15(1):53–8. [PubMed: 30315270]
18. Reichard P. Interactions between deoxyribonucleotide and DNA synthesis. Annu Rev Biochem. 1988;57:349–74. [PubMed: 3052277]

19. Yamamura T, Narumi K, Ohata T, Satoh H, Mori T, Furugen A, et al. Characterization of deoxyribonucleoside transport mediated by concentrative nucleoside transporters. Biochem Biophys Res Commun. 2021 Jun 18;558:120–5. [PubMed: 33910126]
20. Vickers MF, Kumar R, Visser F, Zhang J, Charania J, Raborn RT, et al. Comparison of the interaction of uridine, cytidine, and other pyrimidine nucleoside analogues with recombinant human equilibrative nucleoside transporter 2 (hENT2) produced in Saccharomyces cerevisiae. Biochem Cell Biol Biochim Biol Cell. 2002;80(5):639–44.
21. Toy G, Austin WR, Liao HI, Cheng D, Singh A, Campbell DO, et al. Requirement for deoxycytidine kinase in T and B lymphocyte development. Proc Natl Acad Sci U S A. 2010 Mar 23;107(12):5551–6. [PubMed: 20080663]
22. Arnér ES, Eriksson S. Mammalian deoxyribonucleoside kinases. Pharmacol Ther. 1995;67(2):155–86. [PubMed: 7494863]
23. Radu CG, Shu CJ, Nair-Gill E, Shelly SM, Barrio JR, Satyamurthy N, et al. Molecular imaging of lymphoid organs and immune activation by positron emission tomography with a new [18F]-labeled 2'-deoxycytidine analog. Nat Med. 2008 Jul;14(7):783–8. [PubMed: 18542051]
24. Kim W, Le TM, Wei L, Poddar S, Bazzy J, Wang X, et al. [18F]CFA as a clinically translatable probe for PET imaging of deoxycytidine kinase activity. Proc Natl Acad Sci U S A. 2016 Apr 12;113(15):4027–32. [PubMed: 27035974]
25. Song D, Wang Y, Zhu K, Tian L, Gao Q, Zhou J, et al. DCK is a promising prognostic biomarker and correlated with immune infiltrates in hepatocellular carcinoma. World J Surg Oncol. 2020 Jul 20;18(1):176. [PubMed: 32690026]
26. Nathanson DA, Armijo AL, Tom M, Li Z, Dimitrova E, Austin WR, et al. Co-targeting of convergent nucleotide biosynthetic pathways for leukemia eradication. J Exp Med. 2014 Mar 10;211(3):473–86. [PubMed: 24567448]
27. Bunimovich YL, Nair-Gill E, Riedinger M, McCracken MN, Cheng D, McLaughlin J, et al. Deoxycytidine kinase augments ATM-Mediated DNA repair and contributes to radiation resistance. PloS One. 2014;9(8):e104125.
28. Yang C, Lee M, Hao J, Cui X, Guo X, Smal C, et al. Deoxycytidine kinase regulates the G2/M checkpoint through interaction with cyclin-dependent kinase 1 in response to DNA damage. Nucleic Acids Res. 2012 Oct;40(19):9621–32. [PubMed: 22850745]
29. Beyaert M, Starczewska E, Van Den Neste E, Bontemps F. A crucial role for ATR in the regulation of deoxycytidine kinase activity. Biochem Pharmacol. 2016 Jan 15;100:40–50. [PubMed: 26620371]
30. Austin WR, Armijo AL, Campbell DO, Singh AS, Hsieh T, Nathanson D, et al. Nucleoside salvage pathway kinases regulate hematopoiesis by linking nucleotide metabolism with replication stress. J Exp Med. 2012 Nov 19;209(12):2215–28. [PubMed: 23148236]
31. Nair-Gill E, Wiltzius SM, Wei XX, Cheng D, Riedinger M, Radu CG, et al. PET probes for distinct metabolic pathways have different cell specificities during immune responses in mice [Internet]. American Society for Clinical Investigation; 2010 [cited 2021 Nov 10]. Available from: https://www.jci.org/articles/view/41250/pdf
32. Salas JR, Chen BY, Wong A, Cheng D, Van Arnam JS, Witte ON, et al. 18F-FAC PET Selectively Images Liver-Infiltrating CD4 and CD8 T Cells in a Mouse Model of Autoimmune Hepatitis. J Nucl Med. 2018 Oct;59(10):1616–23. [PubMed: 29700125]
33. Brewer S, Nair-Gill E, Wei B, Chen L, Li X, Riedinger M, et al. Epithelial uptake of [18F]1-(2'-deoxy-2'-arabinofuranosyl) cytosine indicates intestinal inflammation in mice. Gastroenterology. 2010 Apr;138(4):1266–75. [PubMed: 20080095]
34. Chen BY, Ghezzi C, Villegas B, Quon A, Radu CG, Witte ON, et al. 18F-FAC PET Visualizes Brain-Infiltrating Leukocytes in a Mouse Model of Multiple Sclerosis. J Nucl Med. 2020 May;61(5):757–63. [PubMed: 31653711]
35. Tsang JE, Urner LM, Kim G, Chow K, Baufeld L, Faull K, et al. Development of a Potent Brain-Penetrant EGFR Tyrosine Kinase Inhibitor against Malignant Brain Tumors. ACS Med Chem Lett. 2020 Oct 8;11(10):1799–809. [PubMed: 33062157]

36. Fox JJ, Navarro HI, Hashimoto T, Garcia AJ, Goldstein AS. Mass cytometry reveals species-specific differences and a new level of complexity for immune cells in the prostate. Am J Clin Exp Urol. 2019;7(4):281–96. [PubMed: 31511834]
37. Glatigny S, Bettelli E. Experimental Autoimmune Encephalomyelitis (EAE) as Animal Models of Multiple Sclerosis (MS). Cold Spring Harb Perspect Med. 2018 Nov 1;8(11).
38. Lyons JA, San M, Happ MP, Cross AH. B cells are critical to induction of experimental allergic encephalomyelitis by protein but not by a short encephalitogenic peptide. Eur J Immunol. 1999 Nov;29(11):3432–9. [PubMed: 10556797]
39. Murphy JM, Armijo AL, Nomme J, Lee CH, Smith QA, Li Z, et al. Development of new deoxycytidine kinase inhibitors and noninvasive in vivo evaluation using positron emission tomography. J Med Chem. 2013 Sep 12;56(17):6696–708. [PubMed: 23947754]
40. Poddar S, Capparelli EV, Rosser EW, Gipson RM, Wei L, Le T, et al. Development and preclinical pharmacology of a novel dCK inhibitor, DI-87. Biochem Pharmacol. 2020 Feb;172:113742. [PubMed: 31812677]
41. Whitacre CC, Dowdell K, Griffin AC. Neuroendocrine influences on experimental autoimmune encephalomyelitis. Ann N Y Acad Sci. 1998 May 1;840:705–16. [PubMed: 9629297]
42. Leuenberger T, Paterka M, Reuter E, Herz J, Niesner RA, Radbruch H, et al. The role of CD8+ T cells and their local interaction with CD4+ T cells in myelin oligodendrocyte glycoprotein35–55-induced experimental autoimmune encephalomyelitis. J Immunol Baltim Md 1950. 2013 Nov 15;191(10):4960–8.
43. Saligrama N, Zhao F, Sikora MJ, Serratelli WS, Fernandes RA, Louis DM, et al. Opposing T cell responses in experimental autoimmune encephalomyelitis. Nature. 2019 Aug;572(7770):481–7. [PubMed: 31391585]
44. Van Gassen S, Callebaut B, Van Helden MJ, Lambrecht BN, Demeester P, Dhaene T, et al. FlowSOM: Using self-organizing maps for visualization and interpretation of cytometry data. Cytom Part J Int Soc Anal Cytol. 2015 Jul;87(7):636–45.
45. Tusher VG, Tibshirani R, Chu G. Significance analysis of microarrays applied to the ionizing radiation response. Proc Natl Acad Sci U S A. 2001 Apr 24;98(9):5116–21. [PubMed: 11309499]
46. Zhornitsky S, Johnson TA, Metz LM, Weiss S, Yong VW. Prolactin in combination with interferon-β reduces disease severity in an animal model of multiple sclerosis. J Neuroinflammation. 2015 Mar 19;12:55. [PubMed: 25889599]
47. Aharoni R, Eilam R, Stock A, Vainshtein A, Shezen E, Gal H, et al. Glatiramer acetate reduces Th-17 inflammation and induces regulatory T-cells in the CNS of mice with relapsing-remitting or chronic EAE. J Neuroimmunol. 2010 Aug 25;225(1–2):100–11. [PubMed: 20554028]
48. Aharoni R, Herschkovitz A, Eilam R, Blumberg-Hazan M, Sela M, Bruck W, et al. Demyelination arrest and remyelination induced by glatiramer acetate treatment of experimental autoimmune encephalomyelitis. Proc Natl Acad Sci U S A. 2008 Aug 12;105(32):11358–63.
49. Bonfiglio T, Olivero G, Merega E, Di Prisco S, Padolecchia C, Grilli M, et al. Prophylactic versus Therapeutic Fingolimod: Restoration of Presynaptic Defects in Mice Suffering from Experimental Autoimmune Encephalomyelitis. PloS One. 2017;12(1):e0170825.
50. Lee DH, Seubert S, Huhn K, Brecht L, Rötger C, Waschbisch A, et al. Fingolimod effects in neuroinflammation: Regulation of astroglial glutamate transporters? PloS One. 2017;12(3):e0171552.
51. Inoue M, Williams KL, Oliver T, Vandenabeele P, Rajan JV, Miao EA, et al. Interferon-β therapy against EAE is effective only when development of the disease depends on the NLRP3 inflammasome. Sci Signal. 2012 May 22;5(225):ra38.
52. Galligan CL, Pennell LM, Murooka TT, Baig E, Majchrzak-Kita B, Rahbar R, et al. Interferon-beta is a key regulator of proinflammatory events in experimental autoimmune encephalomyelitis. Mult Scler Houndmills Basingstoke Engl. 2010 Dec;16(12):1458–73.
53. Axtell RC, de Jong BA, Boniface K, van der Voort LF, Bhat R, De Sarno P, et al. T helper type 1 and 17 cells determine efficacy of interferon-beta in multiple sclerosis and experimental encephalomyelitis. Nat Med. 2010 Apr;16(4):406–12. [PubMed: 20348925]

54. Aharoni R, Schottlender N, Bar-Lev DD, Eilam R, Sela M, Tsoory M, et al. Cognitive impairment in an animal model of multiple sclerosis and its amelioration by glatiramer acetate. Sci Rep. 2019 Mar 11;9(1):4140. [PubMed: 30858445]
55. Häusler D, Hajiyeva Z, Traub JW, Zamvil SS, Lalive PH, Brück W, et al. Glatiramer acetate immune modulates B-cell antigen presentation in treatment of MS. Neurol Neuroimmunol Neuroinflammation. 2020 May;7(3):e698.
56. Rossi S, Lo Giudice T, De Chiara V, Musella A, Studer V, Motta C, et al. Oral fingolimod rescues the functional deficits of synapses in experimental autoimmune encephalomyelitis. Br J Pharmacol. 2012 Feb;165(4):861–9. [PubMed: 21740406]
57. Seki N, Maeda Y, Kataoka H, Sugahara K, Sugita T, Chiba K. Fingolimod (FTY720) ameliorates experimental autoimmune encephalomyelitis (EAE). Inflamm Regen. 2010;30(6):542–8.
58. Schilling S, Goelz S, Linker R, Luehder F, Gold R. Fumaric acid esters are effective in chronic experimental autoimmune encephalomyelitis and suppress macrophage infiltration. Clin Exp Immunol. 2006 Jul;145(1):101–7. [PubMed: 16792679]
59. Chen H, Assmann JC, Krenz A, Rahman M, Grimm M, Karsten CM, et al. Hydroxycarboxylic acid receptor 2 mediates dimethyl fumarate's protective effect in EAE. J Clin Invest. 2014 May;124(5):2188–92. [PubMed: 24691444]
60. Linker RA, Lee DH, Ryan S, van Dam AM, Conrad R, Bista P, et al. Fumaric acid esters exert neuroprotective effects in neuroinflammation via activation of the Nrf2 antioxidant pathway. Brain J Neurol. 2011 Mar;134(Pt 3):678–92.
61. Safavi F, Thome R, Li Z, Zhang GX, Rostami A. Dimethyl fumarate suppresses granulocyte macrophage colony-stimulating factor-producing Th1 cells in CNS neuroinflammation. Neurol Neuroimmunol Neuroinflammation. 2020 Jul;7(4):e729.
62. Schulze-Topphoff U, Varrin-Doyer M, Pekarek K, Spencer CM, Shetty A, Sagan SA, et al. Dimethyl fumarate treatment induces adaptive and innate immune modulation independent of Nrf2. Proc Natl Acad Sci U S A. 2016 Apr 26;113(17):4777–82. [PubMed: 27078105]
63. Kihara Y, Groves A, Rivera RR, Chun J. Dimethyl fumarate inhibits integrin α4 expression in multiple sclerosis models. Ann Clin Transl Neurol. 2015 Oct;2(10):978–83. [PubMed: 26478898]
64. Klotz L, Eschborn M, Lindner M, Liebmann M, Herold M, Janoschka C, et al. Teriflunomide treatment for multiple sclerosis modulates T cell mitochondrial respiration with affinity-dependent effects. Sci Transl Med. 2019 May 1;11(490):eaao5563.
65. Janssen A, Fiebiger S, Bros H, Hertwig L, Romero-Suarez S, Hamann I, et al. Treatment of Chronic Experimental Autoimmune Encephalomyelitis with Epigallocatechin-3-Gallate and Glatiramer Acetate Alters Expression of Heme-Oxygenase-1. PloS One. 2015;10(6):e0130251.
66. Di Dario M, Colombo E, Govi C, De Feo D, Messina MJ, Romeo M, et al. Myeloid cells as target of fingolimod action in multiple sclerosis. Neurol Neuroimmunol Neuroinflammation. 2015 Dec;2(6):e157.
67. Yoshida Y, Mikami N, Tsuji T, Takada Y, Nakazawa Y, Dan R, et al. Mechanism of induction of immune tolerance in experimental autoimmune encephalomyelitis by combination treatment with fingolimod plus pathogenic autoantigen. Clin Exp Neuroimmunol. 2015;6(1):49–56.
68. Parodi B, Rossi S, Morando S, Cordano C, Bragoni A, Motta C, et al. Fumarates modulate microglia activation through a novel HCAR2 signaling pathway and rescue synaptic dysregulation in inflamed CNS. Acta Neuropathol (Berl). 2015 Aug;130(2):279–95. [PubMed: 25920452]
69. Thiele Née Schrewe L, Guse K, Tietz S, Remlinger J, Demir S, Pedreiturria X, et al. Functional relevance of the multi-drug transporter abcg2 on teriflunomide therapy in an animal model of multiple sclerosis. J Neuroinflammation. 2020 Jan 8;17(1):9. [PubMed: 31915017]
70. Chang JT. Pathophysiology of Inflammatory Bowel Diseases. N Engl J Med. 2020 Dec 31;383(27):2652–64. [PubMed: 33382932]
71. Tsokos GC. Autoimmunity and organ damage in systemic lupus erythematosus. Nat Immunol. 2020 Jun;21(6):605–14. [PubMed: 32367037]

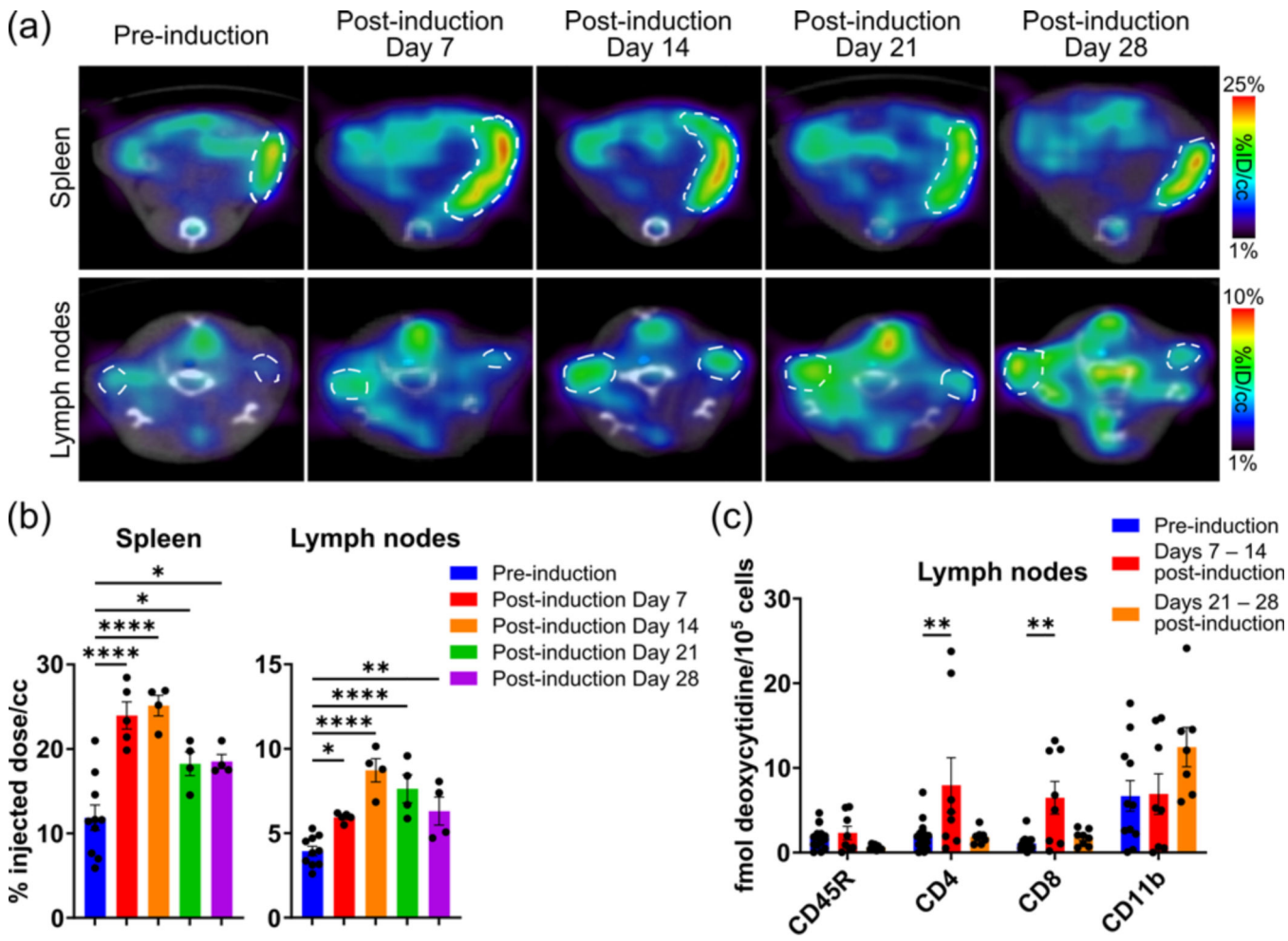

Fig. 1: Deoxyribonucleoside salvage is upregulated in the spleen and lymph nodes throughout disease in $MOG_{35–55}$ EAE mice.

(a) Representative transverse PET/CT images and **(b)** quantification of [^{18}F]FAC accumulation in the spleen and lymph nodes of EAE mice pre- and post-induction. Spleens and lymph nodes encircled in a white dotted line. **(c)** *Ex vivo* accumulation of deoxycytidine in immune cells isolated from the lymph nodes of EAE mice pre- and post-induction. Data in this and subsequent figures represent mean ± SEM. *: P<0.05; **: P<0.01; ****: P<0.0001.

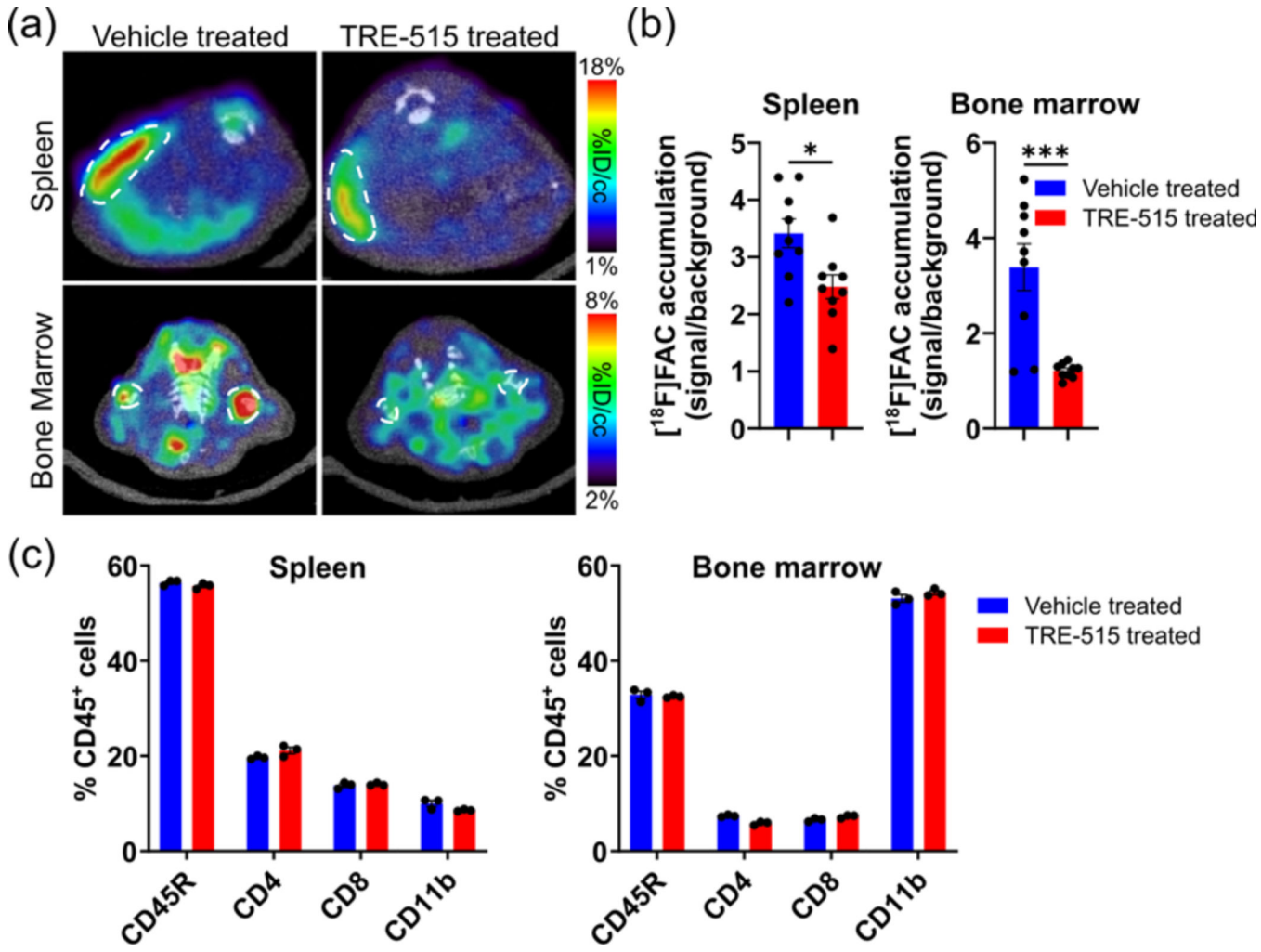

Fig. 2: TRE-515 blocks deoxyribonucleoside salvage activity in the spleen and bone marrow.

(a) Representative transverse PET/CT images and **(b)** quantification of [^{18}F]FAC accumulation in the spleen and bone marrow of mice treated with vehicle or TRE-515 (150 mg/kg QD). Spleens and bone marrow encircled in a white dotted line. **(c)** Percent of CD45^{+} cells for each major immune cell class in the spleen and bone marrow of mice treated with vehicle or TRE-515 (150 mg/kg QD). *: P<0.05; ***P<0.001.

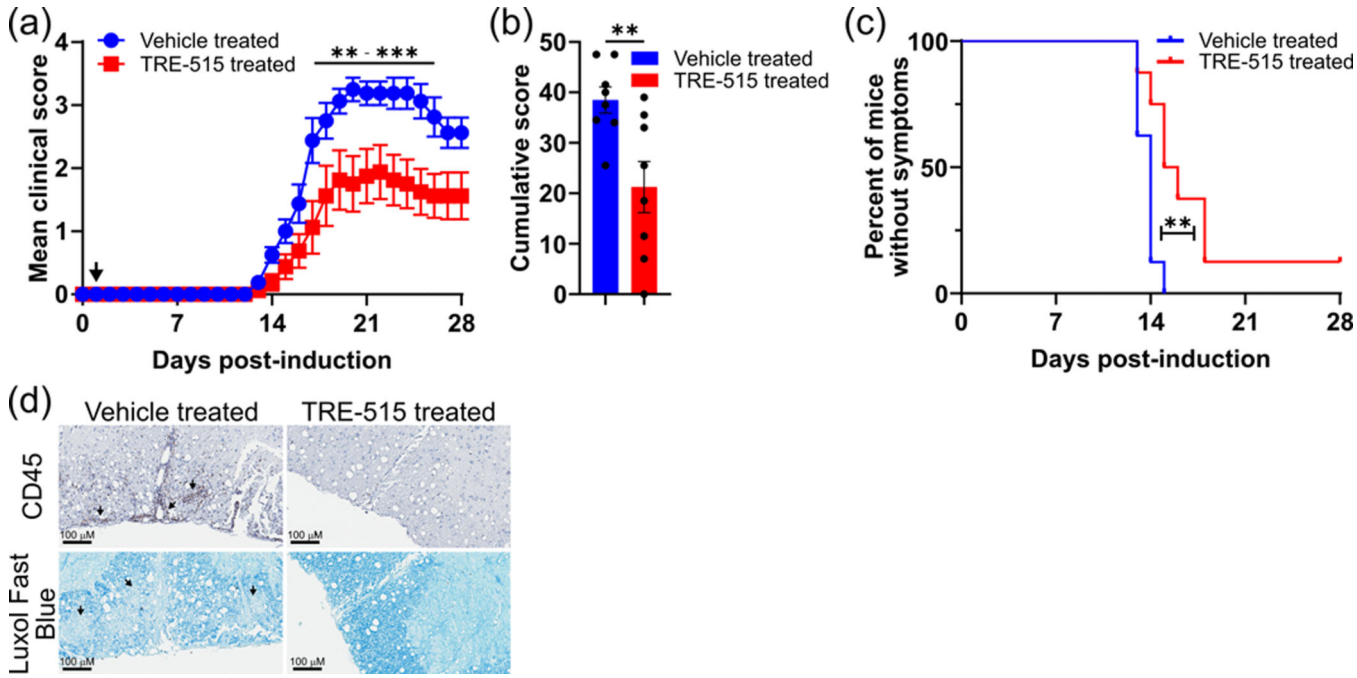

Fig. 3: TRE-515 limits clinical symptoms in $MOG_{35–55}$ EAE mice when treatments are started at disease induction.

(a) Mean clinical score, **(b)** cumulative score, and **(c)** percent of mice without symptoms in $MOG_{35–55}$ EAE mice treated with vehicle or TRE-515 (150 mg/kg QD) starting on Day 1 post-EAE induction. Arrow denotes time point when treatments were initiated. **(d)** Spinal cord sections from Day 21 post-induction EAE mice treated with vehicle or TRE-515 (150 mg/kg QD) starting on Day 1 post-EAE induction stained with a CD45 antibody (*top*) or with Luxol fast blue (*bottom*) to detect myelin. Arrows denote areas of significant leukocyte infiltration or demyelination. **: P<0.01; ***: P<0.001.

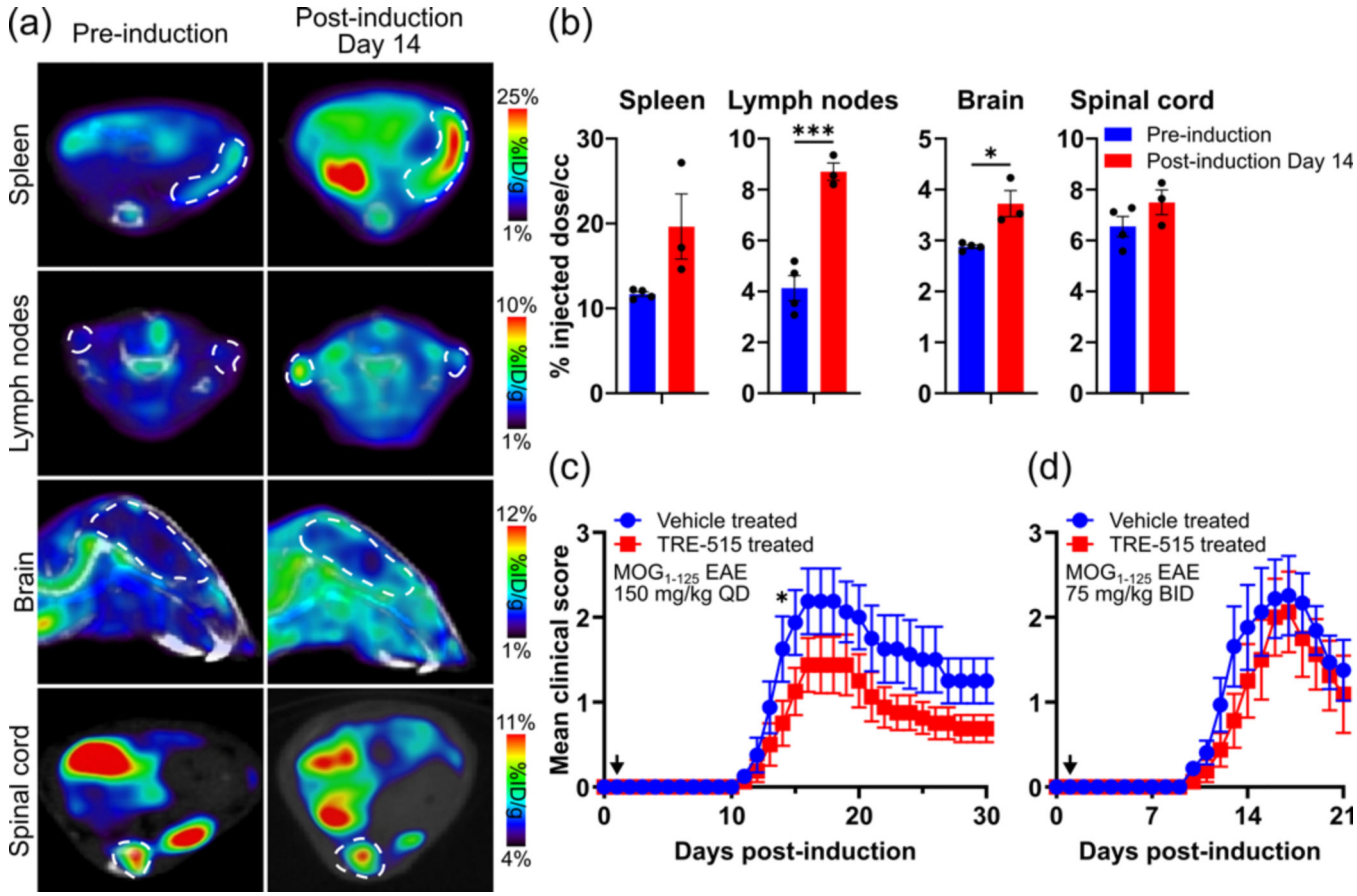

Fig. 4: Deoxyribonucleoside salvage is upregulated and TRE-515 blocks clinical symptoms in $MOG_{1–125}$ EAE mice.

(a) Representative transverse PET/CT images and **(b)** quantification of [^{18}F]FAC accumulation in the spleen, lymph nodes, brain, and spinal cord of $MOG_{1–125}$ EAE mice pre-induction and 14 days post-induction. Spleens, lymph nodes, brains, and spinal cords encircled in a white dotted line. $MOG_{1–125}$ EAE mice were treated daily with vehicle or **(c)** TRE-515 (150 mg/kg QD) or **(d)** TRE-515 (75 mg/kg BID) starting on Day 1. Arrows denote time point when treatments were started. *: P<0.05; ***: P<0.001.

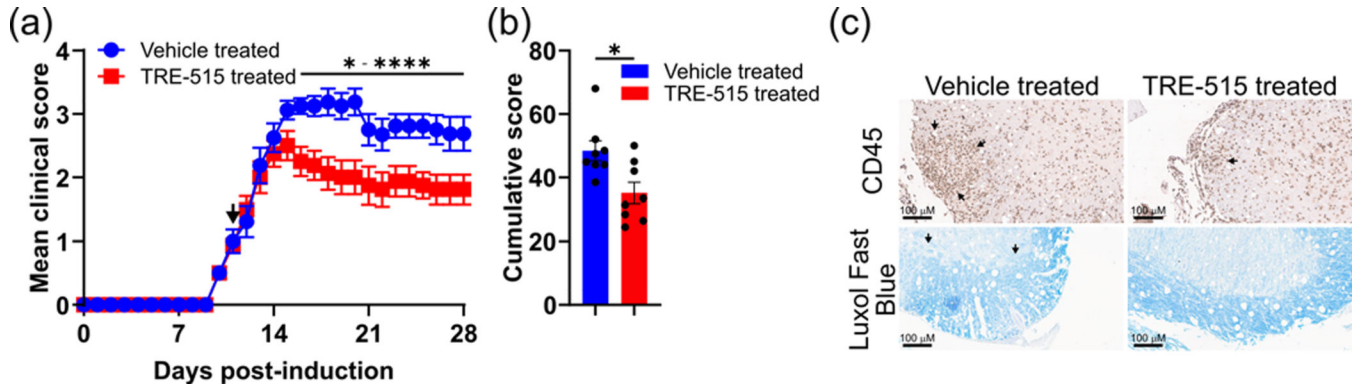

Fig. 5: TRE-515 limits clinical symptoms in $MOG_{35–55}$ EAE mice when treatments are started after the onset of symptoms.

(a) Mean clinical score and **(b)** cumulative score of $MOG_{35–55}$ EAE mice treated with vehicle or TRE-515 (150 mg/kg QD) starting on Day 11 post-EAE induction when all the mice had reached a clinical score of 1 or greater. Arrow denotes time point when treatments were initiated. **(c)** Spinal cord sections from Day 28 post-induction EAE mice treated with vehicle or TRE-515 (150 mg/kg QD) starting at Day 11 post-EAE induction and stained with a CD45 antibody (*top*) or with Luxol fast blue (*bottom*) to detect myelin. Arrows denote areas of significant leukocyte infiltration or demyelination. *: P<0.05; **: P<0.01; ***: P<0.001; ****: P<0.0001.

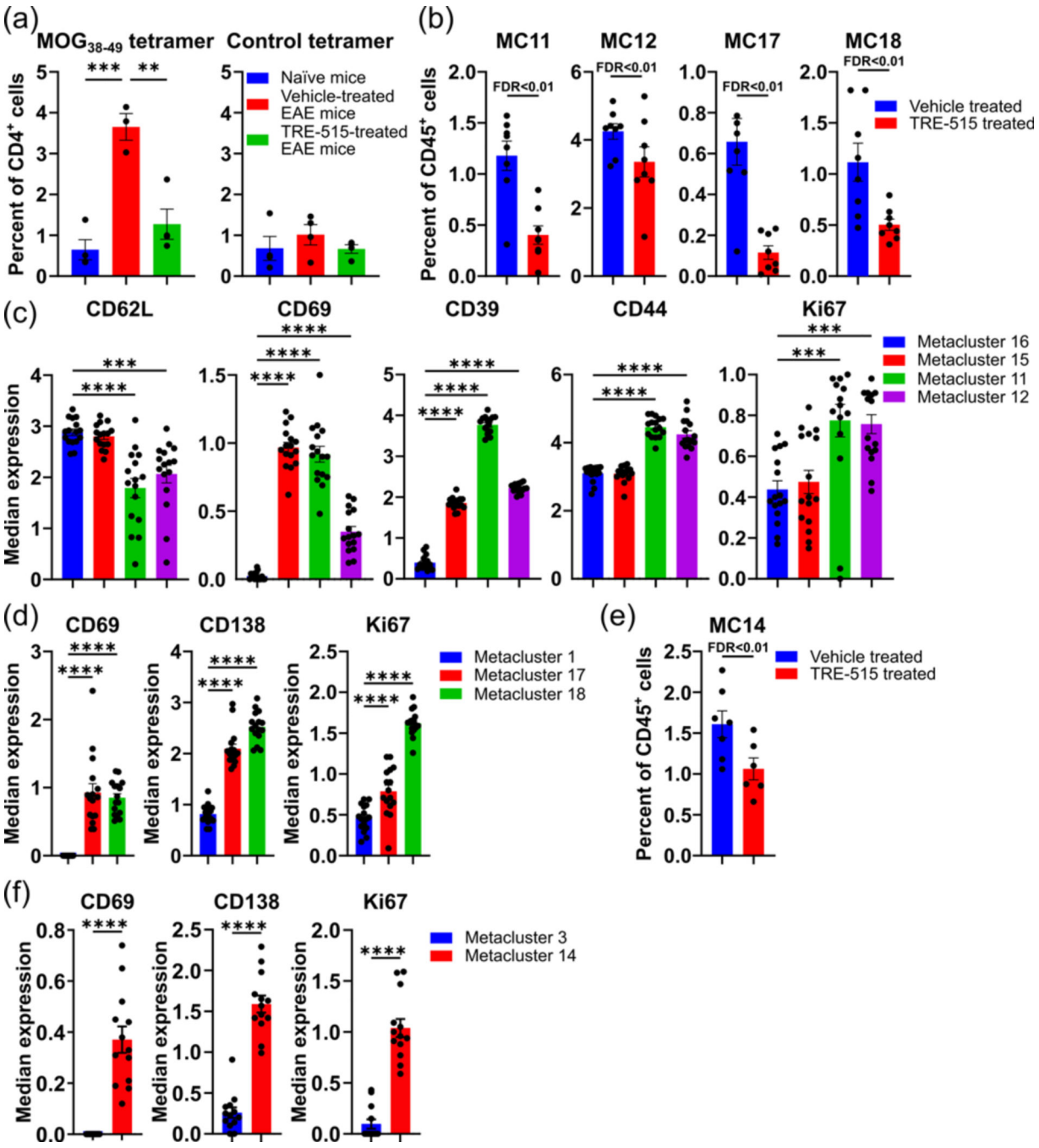

Fig. 6: TRE-515 treatment blocks B and CD4 T cell activation-induced proliferation in EAE mice.

(a) Percent of $MOG_{38–49}$ tetramer and control tetramer stained CD4 T cells in naïve mice, vehicle-treated EAE mice, and TRE-515-treated EAE mice (150 mg/kg QD). In cells from the lymph nodes of EAE mice treated with vehicle or TRE-515 (150 mg/kg QD), 3 days post-induction: **(b)** Metaclusters (MC) for which the percent of cells in that metacluster was significantly affected by the TRE-515 treatment. **(c)** Median expression levels of CD62L, CD69, CD39, CD44, and Ki67 in T cell metaclusters. **(d)** Median expression

levels of CD69, CD138, and Ki67 in B cell metaclusters. In cells from the spleens of EAE mice treated with vehicle or TRE-515 (150 mg/kg QD), 3 days post-induction: **(e)** Metacluster for which the percent of cells in that metacluster was significantly affected by the TRE-515 treatment. **(f)** Median expression levels of CD69, CD138, and Ki67 in the B cell metaclusters. **: P<0.01; ***: P<0.001; ****: P<0.0001.

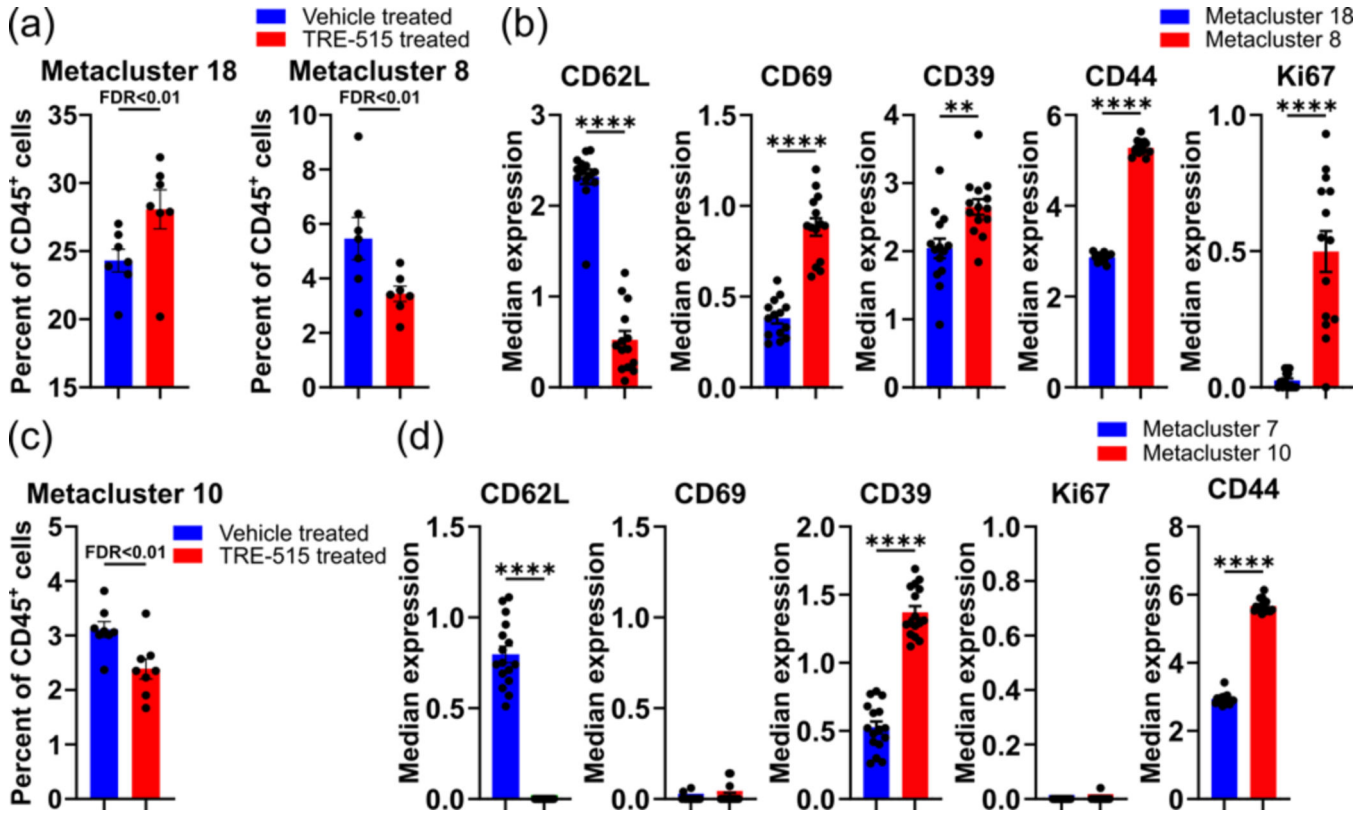

Fig. 7: TRE-515 treatment leads to more naïve CD4 T cells, fewer activated CD4 T cells, and fewer memory CD4 T cells after nine days of treatment.

In cells from the lymph nodes of EAE mice treated with vehicle or TRE-515 (150 mg/kg QD), 10 days post-induction: **(a)** Metaclusters for which the percent of cells in that metacluster was significantly affected by the TRE-515 treatment. **(b)** Median expression levels of CD62L, CD69, CD39, CD44, and Ki67 in CD4 T cell metaclusters. In cells from the spleens of EAE mice treated with vehicle or TRE-515 (150 mg/kg QD), 10 days post-induction: **(c)** Metaclusters for which the percent of cells in that metacluster was significantly affected by the TRE-515 treatment. **(d)** Median expression levels of CD62L, CD69, CD39, Ki67, and CD44 in CD4 T cell metaclusters. **: P<0.01; ****: P<0.0001.

Table 1:

Markers and antibodies used for the CyTOF analyses

Label	Target	Clone	Source
89Y	CD45	30-F11	Fluidigm
115In	Ki67	SolA15	eBioscience
141Pr	TNFα	MP6-XT22	Fluidigm
142Nd	CD39	24DMS1	Fluidigm
143Nd	CD69	H1.2F3	Fluidigm
144Nd	IL2	JES6–5H4	Fluidigm
145Nd	CD4	RM4–5	Biolegend
146Nd	CD150	W19132B	Biolegend
147Sm	CD163	S15049I	Biolegend
149Sm	CD19	6D5	Fluidigm
150Nd	Ly6C	HK1.4	Biolegend
151Eu	Ly6G	1A8	Biolegend
152Sm	CD3e	145–2C11	Fluidigm
153Eu	CD335	29A1.4	Fluidigm
155Gd	CD25	3C7	Biolegend
156Gd	CD14	Sa14–2	Fluidigm
159Tb	TCRγδ	GL3	Fluidigm
160Gd	CD62L	MEL-14	Biolegend
161Dy	iNOS	CXNFT	Fluidigm
162Dy	CD366	RMT3–23	Fluidigm
163Dy	CD138	281–2	Biolegend
164Dy	CD197	4B12	Fluidigm
165Ho	IFNγ	XMG1.2	Biolegend
167Er	GATA3	TWAJ1	Fluidigm
168Er	CD8a	53–6.7	Biolegend
169Tm	TBET	4B10	Biolegend
170Er	CD192	475301R	R&D
171Yb	Granzyme B	QA16A02	Biolegend
172Yb	CD11B	M1/70	Biolegend
173Yb	CD44	IM7	Biolegend
174Yb	MHCII (IA/IE)	M5/114.15.2	Biolegend
175Lu	CD127	A7R34	Biolegend
176Yb	CD45R	RA3–6B2	Biolegend
209Bi	CD11C	N418	Fluidigm